Study of Wind Chill Factor using Infrared Imaging

T. Ahmad*, T. Rashid, H. Khawaja, M. Moatamedi
Faculty of Engineering and Technology, UiT The Arctic University of Norway, Norway

ABSTRACT

This paper presents a study of wind chill factor using infrared imaging. Wind chill factor is the cooling sensation due to the exposure to the wind-temperature environment. The wind chill factor depends on air temperature, wind velocity, and humidity. Wind chill poses serious health risks. Various wind chill index models are presented in the literature. The wind chill factor is closely associated with the phenomenon of heat transfer. The convective mode of heat transfer is most dominant in the case of wind chill.

The paper presents the results of infrared imaging in a controlled environment. The wind drift is recorded experimentally and verified using computational fluid dynamics modelling. The results demonstrated that the rate of heat transfer increases under wind drift. This is evident from the temperature of a human subject captured using infrared imaging.

1. INTRODUCTION

Wind chill factor is explained as the cooling sensation due to the exposure to the wind-temperature environment. An excessive wind chill factor can be a health hazard, since excessive heat loss from the body may result in hypothermia/frostbite [1]. The usual temperature of a human body is 37°C. Heat is generated in the body via metabolic reaction. If heat is withdrawn at a rate higher than it is generated, then hypothermia/frostbite may occur. The same is true in the opposite case: if heat is not withdrawn at an appropriate rate, it may result in hyperthermia/heat stroke. In a cold climate, our bodies create a thin film of heat to keep us warm. This heat film is swept away in windy conditions, hence creating the wind chill factor. This is demonstrated in Figure 1.

The comfort sensation depends on many other variable factors such as temperature, outgoing and incoming radiations, convection and wind velocity, conduction and humidity [2].

The wind chill factor is directly influenced by the phenomenon of heat transfer [3, 4]. Heat transfer is a process of transfer of heat energy from one system to another. Generally, the rate of heat transfer is higher if there is a greater temperature difference between the systems.

One of the earliest wind chill index models was developed by Paul Siple and Charles Passel in 1945 [2, 6]. Their experiment was based on a water-filled plastic container exposed to the cold wind of Antarctica. They recorded the time taken for the water to freeze over a

*Corresponding Author: tah000@post.uit.no

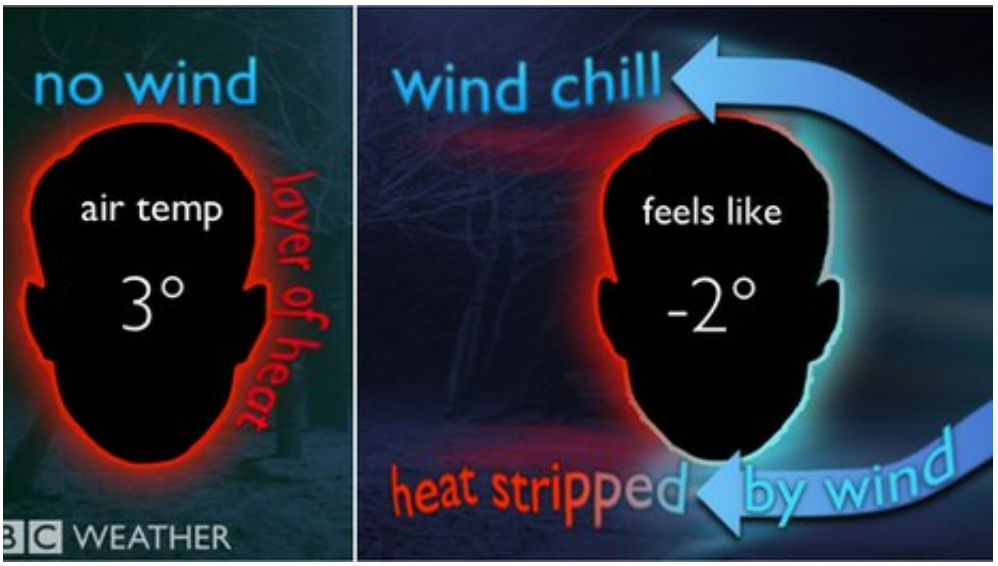

Figure 1: The wind draws heat from the human body creating the wind chill factor [5].

range of temperatures and wind speeds. They used that data to calculate the heat transfer coefficient as shown in Equation (1).

$$h_{wc} = 10.45 + 10V^{\frac{1}{2}} - V \tag{1}$$

where h_{wc} is the heat transfer coefficient in (kCal/m^{2}h°C), and V is wind velocity in m/s. Using Equation (1), they calculated the wind chill index as shown in Equation (2).

$$WCI = h_{wc}(33 - T_{air}) \tag{2}$$

where WCI is an arbitrary wind chill index in (kCal/m^{2}h), T_{air} is the temperature of the surroundings, and it is assumed that the skin temperature is 33°C. WCI was later calibrated against cold sensation such as Cold, Very Cold, Bitterly Cold and Exposed Flesh Freezes. Their model was too crude and suffered serious criticism in the scientific literature [7]. As mentioned in [8], giving the following response, Siple admitted "Looking back, we perhaps made a rather too naïve approach, and we may have made assumptions which were a little careless. However, from a practical standpoint, I think we evolved a scheme that has been of some use."

The Osczevski model considers various parts of the human body and modes of heat transfer [8, 9]. In his studies, heat transfer coefficients were computed for head and face separately, as shown in Equations (3) and (4).

$$h_{head} = 11.5\, V^{0.68} \tag{3}$$

where h_{head} is the head heat transfer coefficient in (W/m^{2}K), and V is wind velocity in m/s.

$$h_{face} = 14.4\ V^{0.61} \tag{4}$$

where h_{face} is the facial heat transfer coefficient in (W/m^{2}K), and V is wind velocity in m/s.

The Osczevski model [8] takes into account the radiative and convective factors of the heat loss, as shown in Equations (5) and (6).

$$h_r = 4\varepsilon\sigma\bar{T}^3 \tag{5}$$

where h_r is the radiative heat transfer coefficient in (W/m^{2}K), ε is the emissivity (estimated to be about 0.04 [10]), σ is the Stefan-Boltzmann constant and $\bar{T}$ is the mean air temperature.

$$h_c = 8.7\ V^{0.6} \tag{6}$$

where h_c is the convective heat transfer coefficient in (W/m^{2}K), and V is wind velocity in m/s.

Osczevski [8] delivered the Wind Chill Index model for facial cooling. His model is based on heat flow per unit area, as shown in Equation (7).

$$Q = \frac{37 - T_{cheek}}{R_{cheek}} \tag{7}$$

where Q is the heat flow per unit area (W/m^2), T_{cheek} is the cheek skin temperature (°C), R_{cheek} is the thermal resistance of skin in (m^{2}K/W), and it is assumed that the core body temperature is 37°C. Using the calculated value of Q, Osczevski's Wind Chill Index for facial cooling can be calculated using Equation (8).

$$WCI = 4.2Q - f(T_{air}) \tag{8}$$

where WCI is the Wind Chill Index (kCal/m^{2}h), and $f(T_{air})$ is a function based on the temperature of the surroundings. Osczevski [8] associated the discomfort descriptor with various values of the Wind Chill Index, as shown in Table 1. In addition, this work also gives a plot of the Wind Chill Index with wind speed for different facial temperatures (shown in Figure 2). These values could be controversial and may be different for each individual [11].

Table 1: Discomfort Descriptor with Wind Chill Index Value [8].

Discomfort Descriptor	Wind Chill Index (kCal/m^{2}h)
Cold	800
Very Cold	1000
Bitterly Cold	1200
Exposed Flesh Freezes	1400

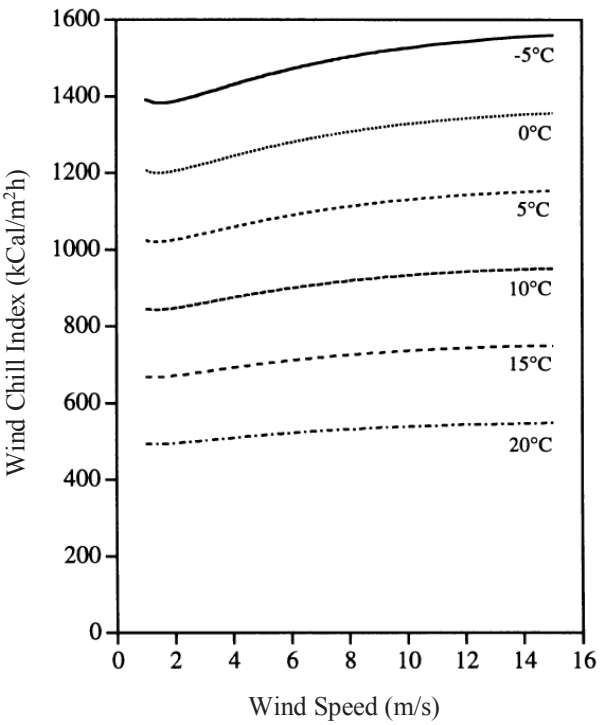

Figure 2: Wind Chill Index (kCal/m^2) with wind speed (m/s) for various facial temperatures ranging from -5°C to 20°C [8].

Osczevski and Bluestein published a new wind chill equivalent chart in 2005 [12]. This model is widely accepted and being used by various meteorological departments around the globe [13]. This model computes the wind chill temperature, also known as the efffective or feels like temperature, from wind speed and surrounding temperature, as shown in Equation (9).

$$WCT = 13.2 + 0.6215\,T_{air} - 11.37\,V_s^{0.16} + 0.3965\,T_{air}\,V_s^{0.16} \quad (9)$$

where WCT is wind chill temperature in (°C), T_{air} is temperature of the surrounding air in (°C), and V_s is the wind speed in (km/h). The results can be plotted in a chart, as shown in Figure 3.

Wind Speed (km h⁻¹) \ Air Temperature (°C)	Calm	10	5	0	−5	−10	−15	−20	−25	−30	−35	−40	−45	−50
10	9	3	−3	9	−15	−21	**−27**	**−33**	**−39**	**−45**	**−51**	**-57**	**−63**
15	8	2	−4	−11	−17	−23	**−29**	**−35**	**−41**	**−48**	**−54**	**−60**	**−66**
20	7	1	−5	−12	−18	−24	**−31**	**−37**	**−43**	**−49**	**−56**	**−62**	**−68**
25	7	1	−6	−12	−19	−25	**−32**	**−38**	**−45**	**−51**	**−57**	**−64**	**−70**
30	7	0	−7	−13	−19	−26	**−33**	**−39**	**−46**	**−52**	**−59**	**−65**	**−72**
35	6	0	−7	−14	−20	−27	**−33**	**−40**	**−47**	**−53**	**−60**	**−66**	**−73**
40	6	−1	−7	−14	−21	**−27**	**−34**	**−41**	**−48**	**−54**	**−61**	**−68**	**−74**
45	6	−1	−8	−15	−21	**−28**	**−35**	**−42**	**−48**	**−55**	**−62**	**-69**	**−75**
50	6	−1	−8	−15	−22	**−29**	**−35**	**−42**	**−49**	**−56**	**−63**	**−70**	**−76**
55	5	−2	−9	−15	−22	**−29**	**−36**	**−43**	**−50**	**−57**	**−63**	**−70**	**−77**
60	5	−2	−9	−16	−23	**−30**	**−37**	**−43**	**−50**	**−57**	**−64**	**−71**	**−78**
70	5	−2	−9	−16	−23	**−30**	**−37**	**−44**	**−51**	**−59**	**−66**	**−73**	**−80**
80	4	−3	−10	−17	−24	**−31**	**−38**	**−45**	**−52**	**−60**	**−67**	**−74**	**−81**

Figure 3: Wind chill temperature (°C) with air temperature (°C) and wind speed (km/h). The shaded region shows when frostbite may occur [12].

Researchers have also argued the merits of wind chill estimation [14].

The objective of this work is to study wind chill effect in a controlled environment (cold room at The Arctic University of Norway). In this work, wind drift is recorded experimentally and verified using computational fluid dynamics (CFD) modeling.

2. METHODOLOGY

2.1 Cold Room

A cold room at The Arctic University of Norway, Tromsø, provides a suitable environment for testing wind chill effect. The dimensions of the room are shown in Figure 5.

The cold room can be set as low as -40°C; however, due to a technical limitation with its cooling system, it is not advisable to maintain this temperature for an extended period of time. The ideal operating condition for the cold room chamber is between -20°C and -25°C. Humidity was kept low to avoid icing over the evaporator blades.

Mounted in the room is an evaporator with two fans, as shown in Figure 5. The evaporator brings into the room coolant, which is circulated by the fans. The fans provide variable wind drift in the room. This wind drift is measured using an anemometer (TSI® Velocicalc® Air Velocity Meter Model 5725) as shown in Figure 4. These are average velocity values.

In order to understand the wind drift in a cold room, a computational fluid dynamics (CFD) model of the cold room was built and analyzed using ANSYS® CFX [16]. Figure 6 shows the finite volume mesh of the cold room. The auto-meshing function was used to generate CFD meshes. Mesh sensitivity analysis was performed to ensure the correctness of the results. K-Epsilon (K- ϵ) turbulence model was used. The boundary layers around the room were not resolved, to conserve the computations. Inlet boundary condition was applied at fan inlets as shown in Figure 7(a). The real time wind velocity was measured using an anemometer (TSI® Velocicalc® Air Velocity Meter Model 5725[15]) and applied as a

Figure 4: TSI® Velocicalc® Air Velocity Meter Model 5725 [15]

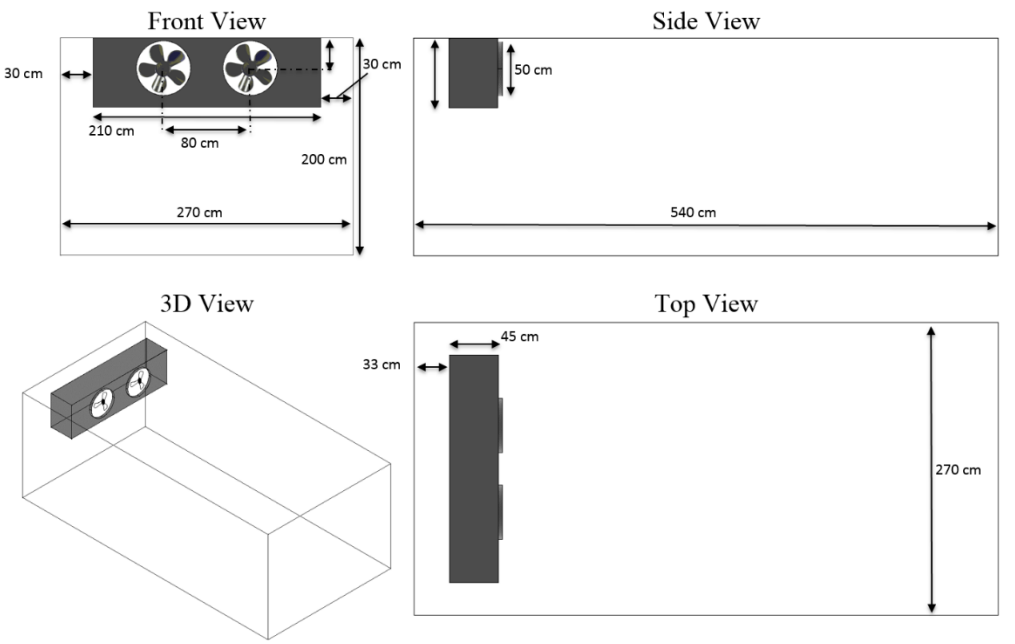

Figure 5: Technical drawings of cold room chamber at the Arctic University of Norway, Tromsø.

boundary condition. This value was found to vary between 8-10 m/s. The constant pressure outlet boundary condition was applied at the inlet of the cooling system as shown in Figure 7(b).

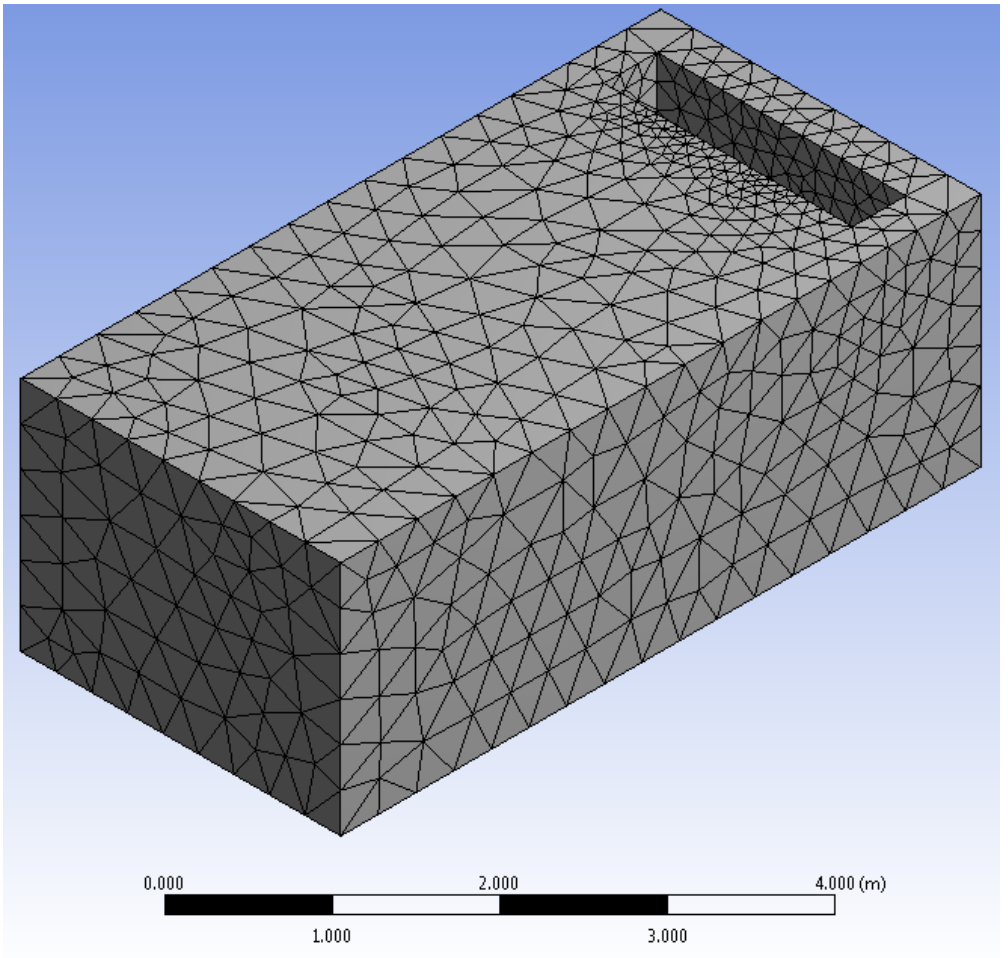

Figure 6: Finite volume mesh of cold room

2.2 Infrared Imaging

In this study, we have used a Fluke® Ti55 IR camera. The camera is shown in Figure 8. Table 2 summarizes the features of the Fluke® Ti55 IR camera. SmartView® image analysis software is used to analyze the data from the Fluke® Ti55 IR camera [17]. The software provides a number of features to analyze the images according to the needs of the user. SmartView® software helps to visualize both the digital and IR images in the same profile, as shown in Figure 9.There are different analysis settings in SmartView® software to change colors, saturation, color alarm, display markers, emissivity settings, and background temperature.

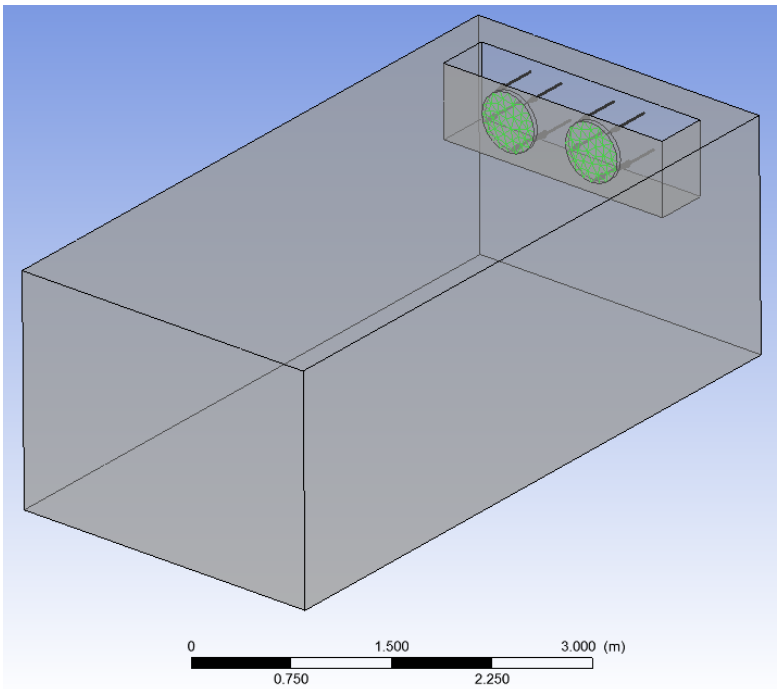

(a)

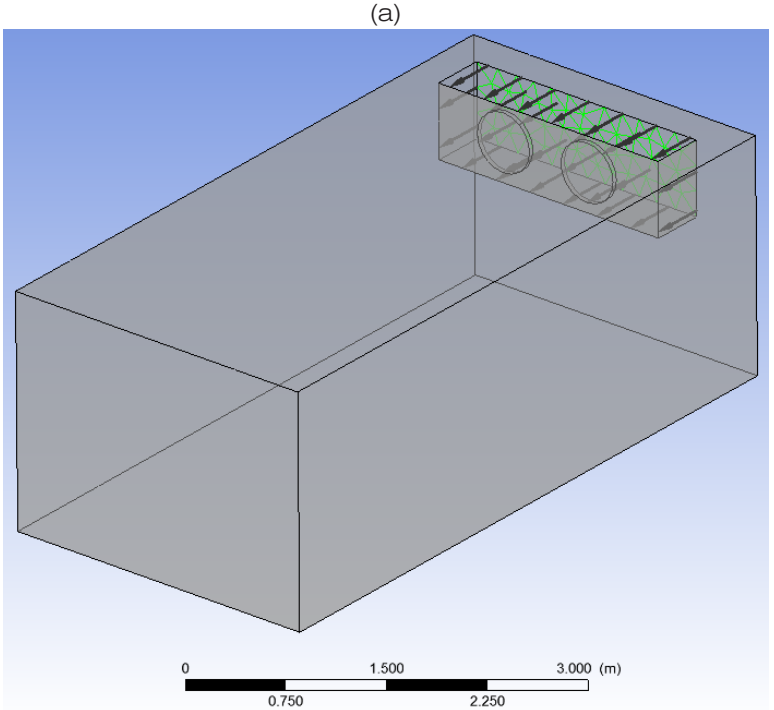

(b)

Figure 7: CFD inlet and outlet boundary conditions of the cold room

Infrared imaging has been used previously for the study of cold objects such as ice [19, 20].

Figure 8: Fluke® Ti55 IR camera

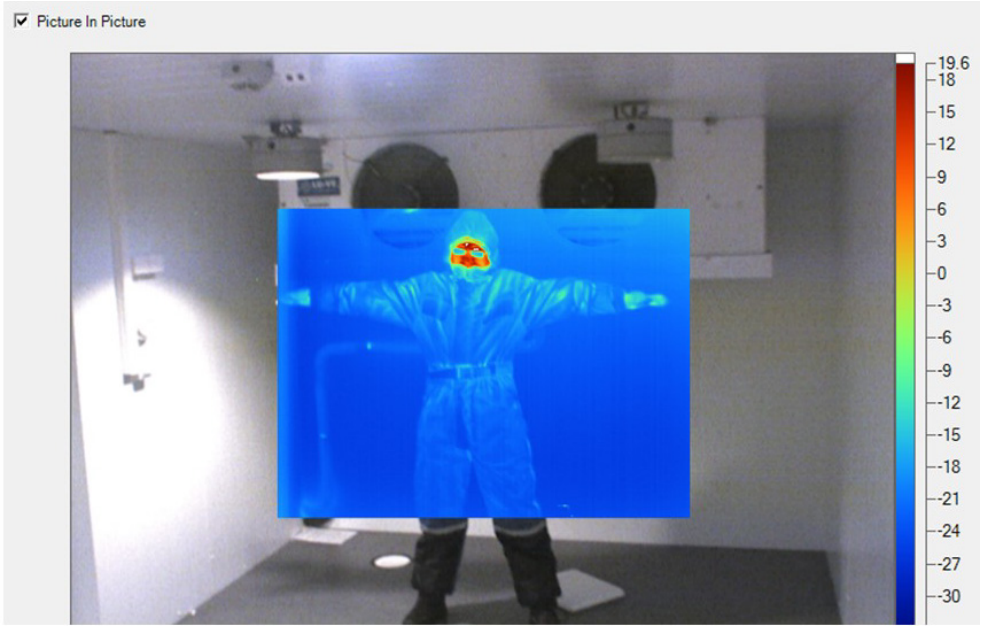

Figure 9: IR image overlapped over the digital image (image was taken in the cold room with Fluke® Ti55 IR camera and analyzed in SmartView® [18]).

Table 2: Features of Fluke® Ti55 IR Camera [17]

Field of View (FOV)	20 mm lens 23° x 17° 10.5 mm lens 42°x 32° 54 mm lens 9° x 6 °
Minimum Focus Distance	Not provided
IR Resolution	320 × 240 pixels
Emissivity Correction	Variable from 0.1 to 1.0
Detector Pitch	25 μm
Spectral Range	8 μm to 14 μm
Temperature Range	– 20°C to +100°C
Accuracy	± 2°C or ± 2% of reading

3. RESULTS AND DISCUSSIONS

3.1 Wind Drift in Cold Room

This wind drift was measured using an anemometer (TSI® Velocicalc® Air Velocity Meter Model 5725 [15]) as shown in Figure 10. These are average velocity values.

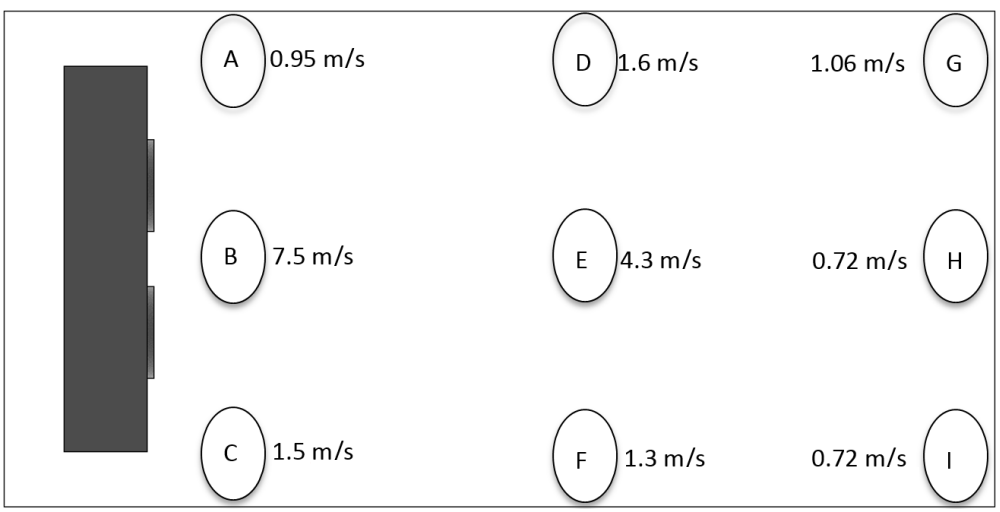

Figure 10: Wind velocities in cold room. The wind velocities were measured using anemometer (TSI® Velocicalc® Air Velocity Meter Model 5725) in the plane horizontal to the fans.

Computational fluid dynamics (CFD) results validated the measured results within reasonable accuracy. The CFD results are shown in Figure 11. Figure 11(a) shows the velocity streamlines in a cold room, while Figure 11(b) shows the velocity contours in the plane horizontal to the fans in the cold room.

3.2 Infrared Imaging Results

In order to see the effect of wind chill, IR images of subjects were taken in a cold room chamber. The subjects were wearing cold protection dress (Figure 12) in order to be safe from any harm

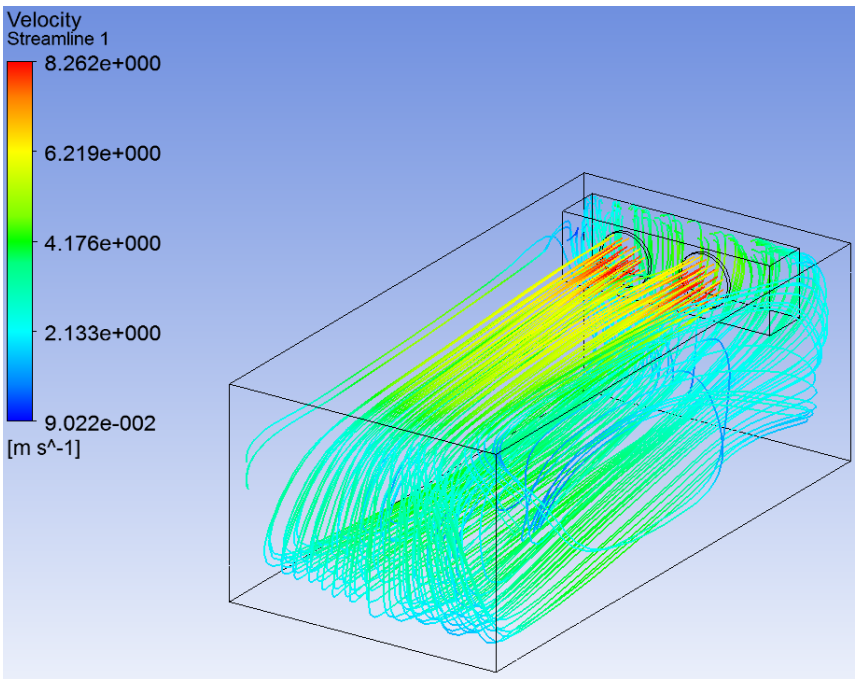

(a)

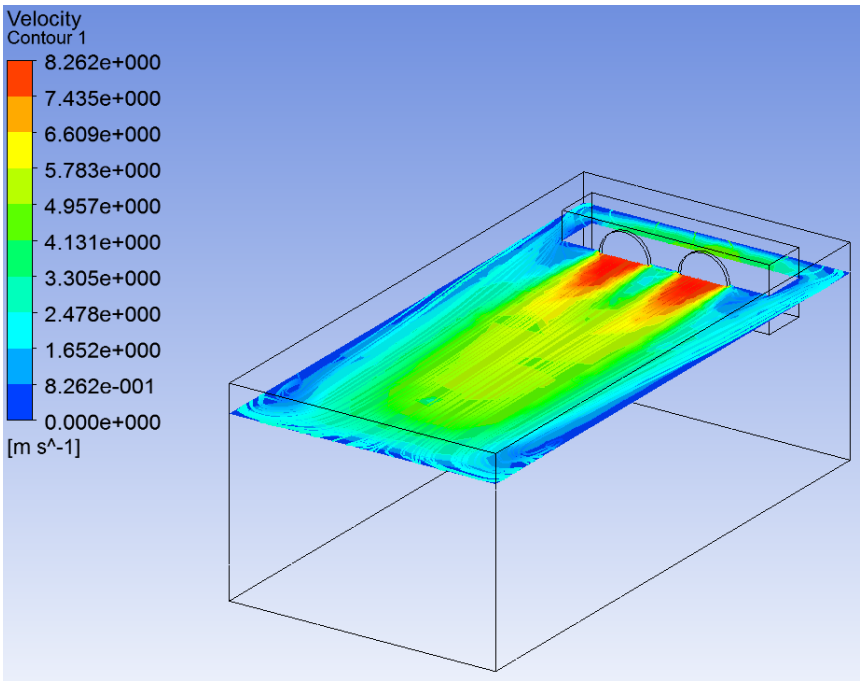

(b)

Figure 11: CFD velocity results of the cold room; (a) velocity streamlines, (b) velocity contours on the plane horizontal to the fans.

during the experiments. The subjects were asked to remain in position for around five minutes before the images were taken.

Figure 12: Subject is wearing cold protection dress. The image was taken in cold room chamber at the Arctic University of Norway, Tromsø.

Due to the limited field of view of the Fluke® Ti55 IR camera (refer to Table 2) [17], the subjects can only be placed at two positions in the cold room. These positions were B and H (refer to Figure 10). The obtained IR images were analyzed in SmartView® software [18]. The results are shown in Figure 13 and Figure 14. It is evident from the images that temperatures were higher at position H in comparison to position B. This is due to the fact that wind velocity was 7.5 m/s at position B and 0.72 m/s at position H. The same result is illustrated by drawing a line from hand-to-hand of Subject 1. The temperature profile clearly indicates the temperature differences. It is shown from Figure 15 that the lower end of the temperature is around -20°C. This value increases to about -18°C in Figure 16. This clearly demonstrates the fact that there

is more heat loss at position B in comparison to position H. During these experiments, the air temperature of the cold room chamber was about -22°C.

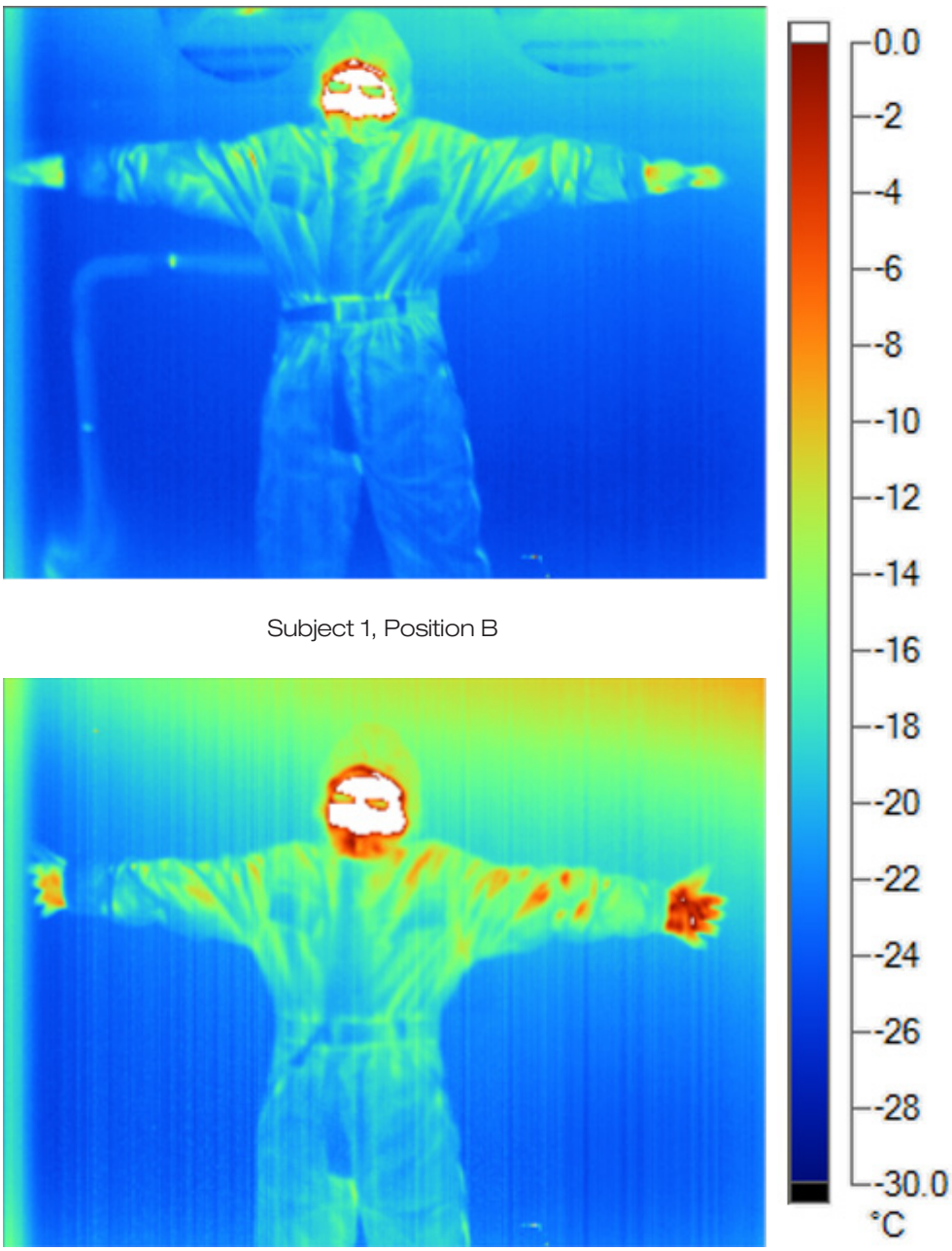

Subject 1, Position B

Subject 1, Position H

Figure 13: IR images of Subject 1 at positions B and H respectively.

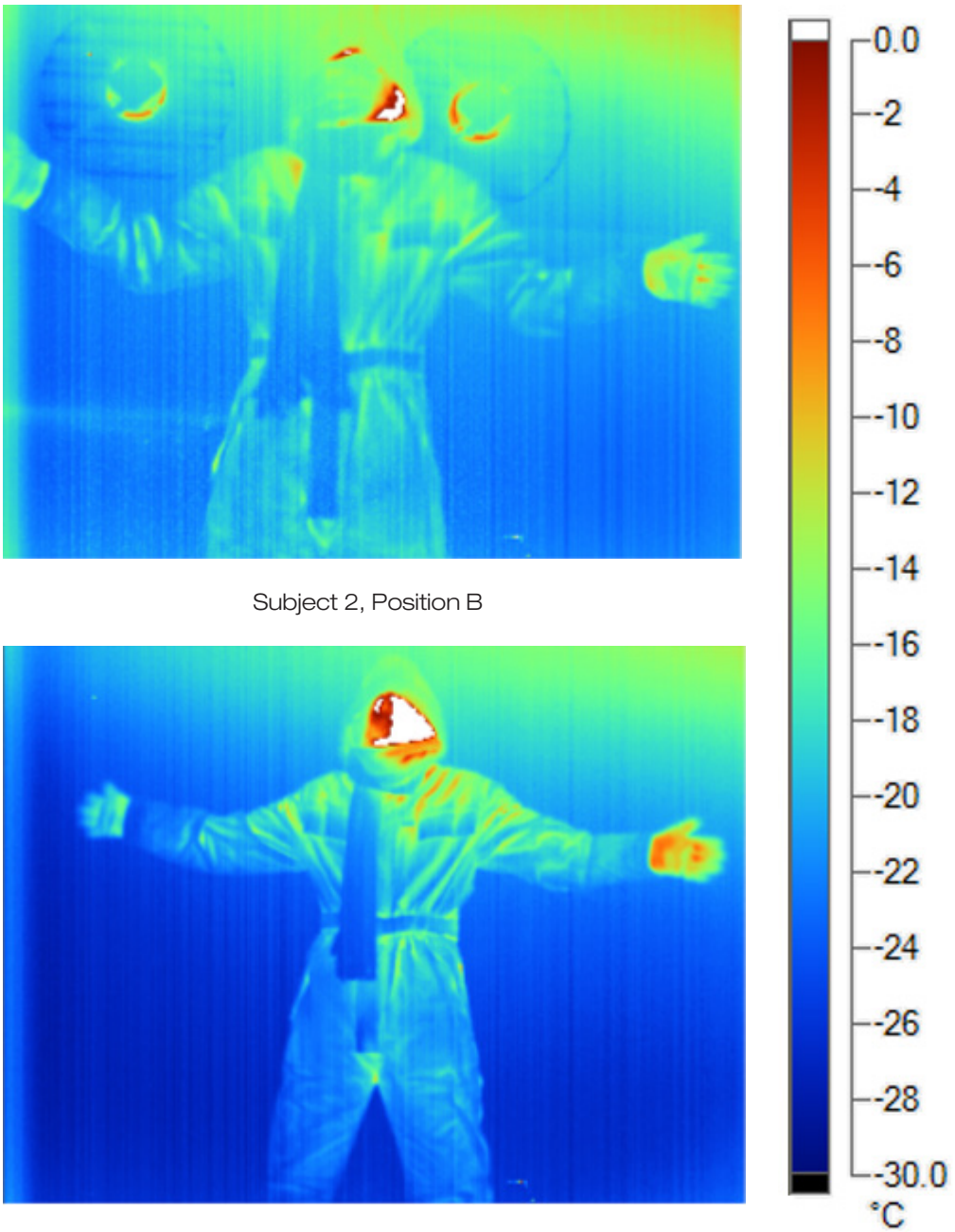

Subject 2, Position B

Subject 2, Position H

Figure 14: IR images of Subject 2 at positions B and H respectively.

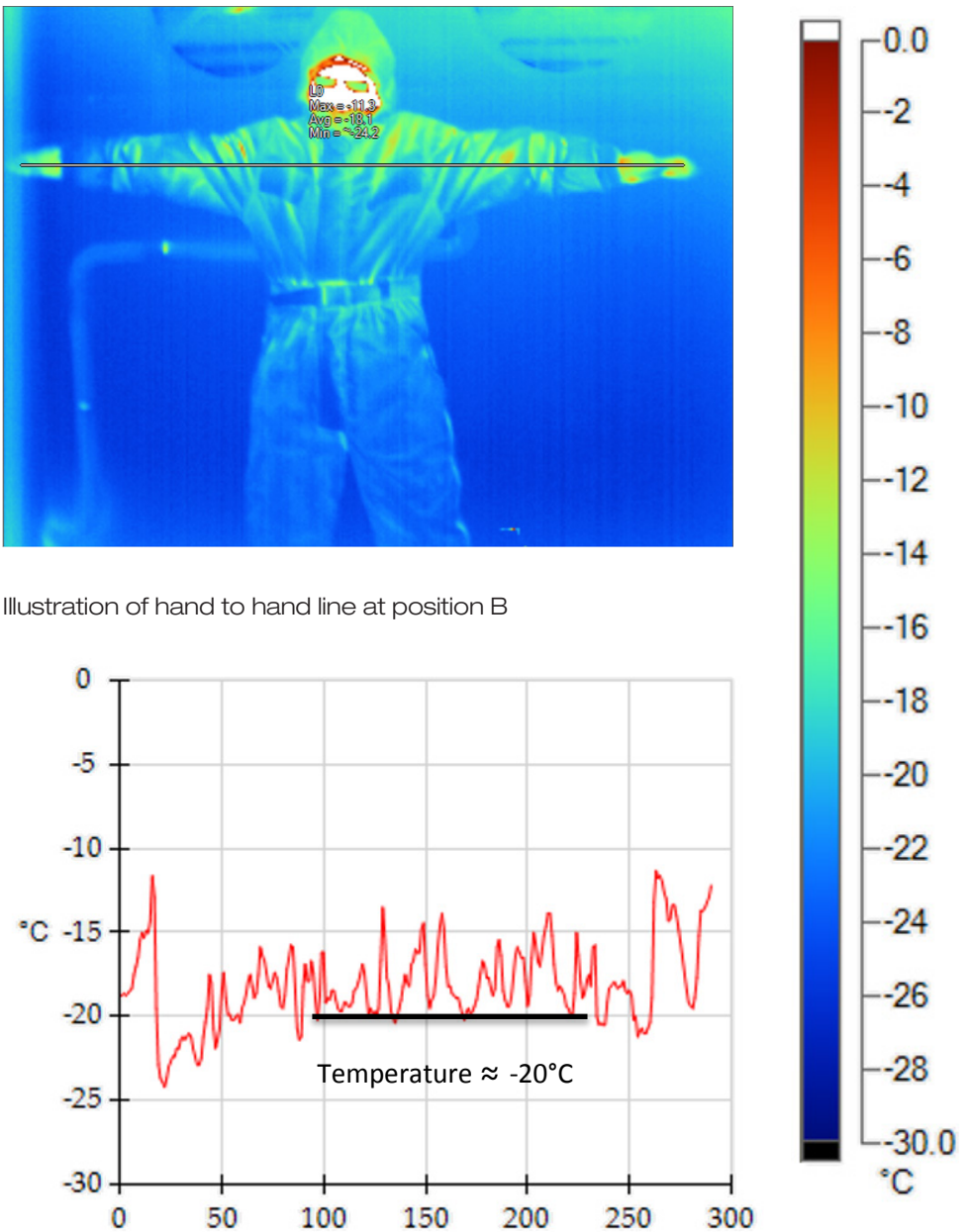

Illustration of hand to hand line at position B

Temperature profile (horizontal axis shows no. of points on the line)

Figure 15: Hand to hand line and temperature profile at position B

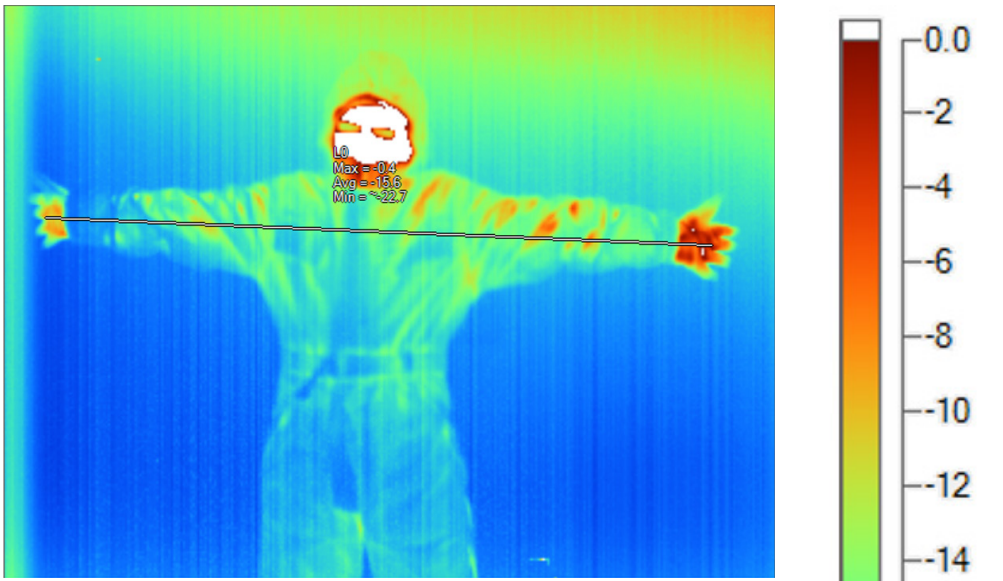

Illustration of hand to hand line at position H

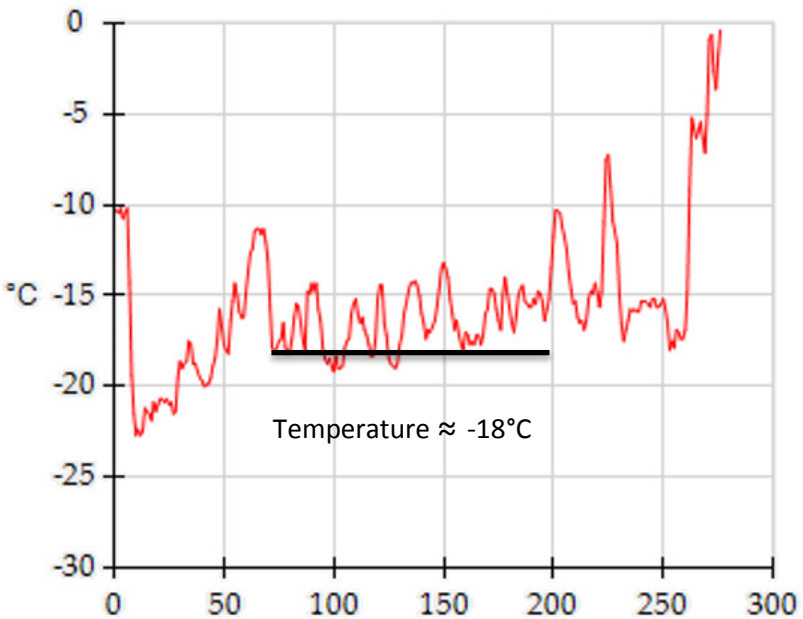

Temperature profile (horizontal axis shows no. of points on the line)

Figure 16: Hand to hand line and temperature profile at position H

4. CONCLUSION

It is evident from the infrared imaging results that the recorded temperatures vary with different wind drifts, even though the surrounding temperature is constant (-22°C). Under higher wind drift, the recorded temperatures are lower and vice versa. This demonstrates that the heat loss is greater when the recorded temperatures are lower. Therefore, higher wind velocity results in higher heat loss and stronger wind chill factor.

ACKNOWLEDGEMENT

The authors would like to acknowledge the support of Mr. Intisab Alam Khan at Department of Engineering and Safety, UiT The Arctic University of Norway, Tromsø, Norway.

REFERENCES:

[1] Wilson, O. Atmospheric cooling and the occurrence of frostbite in exposed skin. In: Proceedings Symposia on Arctic. Medicine and Biology. IV. Frostbite. E. Viereck (ed.), Arctic Aeromedical Laboratory, Fort Wainwright, Alaska. 1964.

[2] Siple, P.A. and C.F. Passel, Measurements of dry atmospheric cooling in subfreezing temperatures. Proceedings of the American Philosophical Society, 1945. 89(1): p. 177-199.

[3] Brauner, N. and M. Shacham, Meaningful wind chill indicators derived from heat transfer principles. International Journal of Biometeorology, 1995. 39(1): p. 46-52.

[4] Steadman, R.G., Indices of windchill of clothed persons. Journal of Applied Meteorology, 1971. 10(4): p. 674-683.

[5] BBC., What is wind chill? 2016 [cited 2016 17-04-2016]; Available from: http://www.bbc.co.uk/weather/feeds/31013287.

[6] Maarouf, A. and M. Bitzos, Windchill indices. A review of science. Current Applications and Future Directions for Canada, 2000.

[7] Molnar, G., An evaluation of wind chill. In: Sixth Conference on Cold Injury 1960, Josiah Macy Foundation: New York. p. 175-221.

[8] Osczevski, R.J., The basis of wind chill. Arctic, 1995: p. 372-382.

[9] Osczevski, R.J., Windward cooling: an overlooked factor in the calculation of wind chill. Bulletin of the American Meteorological Society, 2000. 81(12): p. 2975-2978.

[10] Cain, J. and N. McKay, Thermal radiative properties of metallized films. Journal of Building Physics, 1991. 14(3): p. 221-240.

[11] Rees, W., A new wind-chill nomogram. Polar Record, 1993. 29(170): p. 229-234.

[12] Osczevski, R. and M. Bluestein, The new wind chill equivalent temperature chart. Bulletin of the American Meteorological Society, 2005. 86(10): p. 1453-1458.

[13] YR., Effektiv temperatur. 2012 [cited 2015 14-01-2015]; Available from: http://om.yr.no/forklaring/symbol/effektiv-temperatur/.

[14] Shitzer, A. and P. Tikuisis, Advances, shortcomings, and recommendations for wind chill estimation. International Journal of Biometeorology, 2012. 56(3): p. 495-503.

[15] TSI®, Velocicalc® Air Velocity Meter Model 5725 - Operation and Service Manual 2016.

[16] ANSYS®, CFX (Academic Research). release 16.2.

[17] FLUKE®, Introduction to Thermography Principles 2009.

[18] SmartView®, Infrared Imaging Analysis and Reporting Software 2016: FLUKE®.

[19] Rashid, T., et al., Infrared thermal signature evaluation of a pure and saline ice for marine operations in cold climate. Sensors & Transducers Journal, 2015. 194(11): p. 62-68.

[20] Rashid, T.K., A. Hassan, K. Edvardsen, and U.N. Mughal, Infrared thermal signature evaluation of a pure ice block. In: Sensorcomm 2015. International Academy, Research and Industry Association (IARIA): Venice, Italy.